

Are normal fault earthquakes due to elastic rebound or gravitational collapse?

Christian Bignami¹, Emanuela Valerio², Eugenio Carminati³, Carlo Doglioni^{*,1,3}, Patrizio Petricca³, Pietro Tizzani², Riccardo Lanari²

⁽¹⁾ Istituto Nazionale di Geofisica e Vulcanologia, Rome, Italy

⁽²⁾ National Research Council (CNR), Istituto per il Rilevamento Elettromagnetico dell'Ambiente (IREA), Napoli, Italy

⁽³⁾ Dipartimento di Scienze della Terra, Sapienza University, Rome, Italy

Article history: received March 25, 2020; accepted May 16, 2020

Abstract

We discuss two competing models for explaining the ground deformation associated with normal faulting earthquake in the brittle elastic upper crust. The classic elastic rebound theory is usually applied for all tectonic settings. In normal fault earthquakes, this model would predict a horizontal stretching eventually responsible for the elastic rebound at the earthquake. However, volumes mostly subside vertically during an extensional earthquake and the collapsed ground in the hanging wall is about one order of magnitude larger than the uplifted volumes of the surrounding hanging wall and footwall. The elastic rebound model would explain this asymmetry with a high horizontal elastic compressibility of the hanging wall and footwall absorbing the coseismic push. We rather suggest that the force activating normal fault earthquakes is mostly dictated by the sliding of the hanging wall, owing gravitational potential. The much larger coseismic subsidence with respect to the uplift can be explained by the closure at depth of a diffuse network of microfractures developed during the interseismic period. Since the horizontal stretching does not exist below ~1 km of depth, with the minimum horizontal stress tensor becoming positive below that depth, the development of a normal fault can be activated only by the vertical maximum stress tensor, i.e., the lithostatic load. The common fluids expulsion at the coseismic stage requires diffuse secondary permeability in the upper crust, in agreement with the presence of a diffuse network of microfractures.

Keywords: Normal fault earthquakes; Graviquakes; Lithostatic load; Coseismic deformation; Fluid expulsion.

1. Introduction

The brittle upper crust can be assumed as an elastic medium at the timescale of earthquakes, delivering elastic waves when perturbed instantaneously [e.g., Stein and Wysession, 2009]. Segall and Heimisson [2019] recently suggested that the elastic dislocation theory in extensional tectonic settings does not require a volume collapse at depth, as proposed by Bignami et al. [2019]. Segall and Heimisson [2019] indicate that the common theory of the horizontal elastic rebound reasonably reproduces the observed geodetic data, and infer how the extra coseismically

subsided volume is accommodated by compressibility in the hanging wall. However, their analytical solution fails to answer two fundamental questions about the ground deformation associated with earthquakes in extensional tectonic settings. The first concerns the energy controlling the hanging wall motion; the second where the extra subsided volume would be adsorbed, considering the real mechanical constraints. Valerio et al. [2018] and Bignami et al. [2019] demonstrated that, for the Mw 6.5 central Italy, 2016 earthquake, the coseismically subsided volume is far greater than the uplifted crustal volume (Figure 1), posing the question of where this unbalance is compensated at depth, and what is the energy that can explain the geometry and kinematics of the half-graben (Figure 2). We investigate here the energy source and kinematics of normal fault earthquakes, keeping in mind that the fault plane is only the passive discontinuity along which part of the energy accumulated by the crustal volume during the interseismic period is dissipated at the coseismic stage.

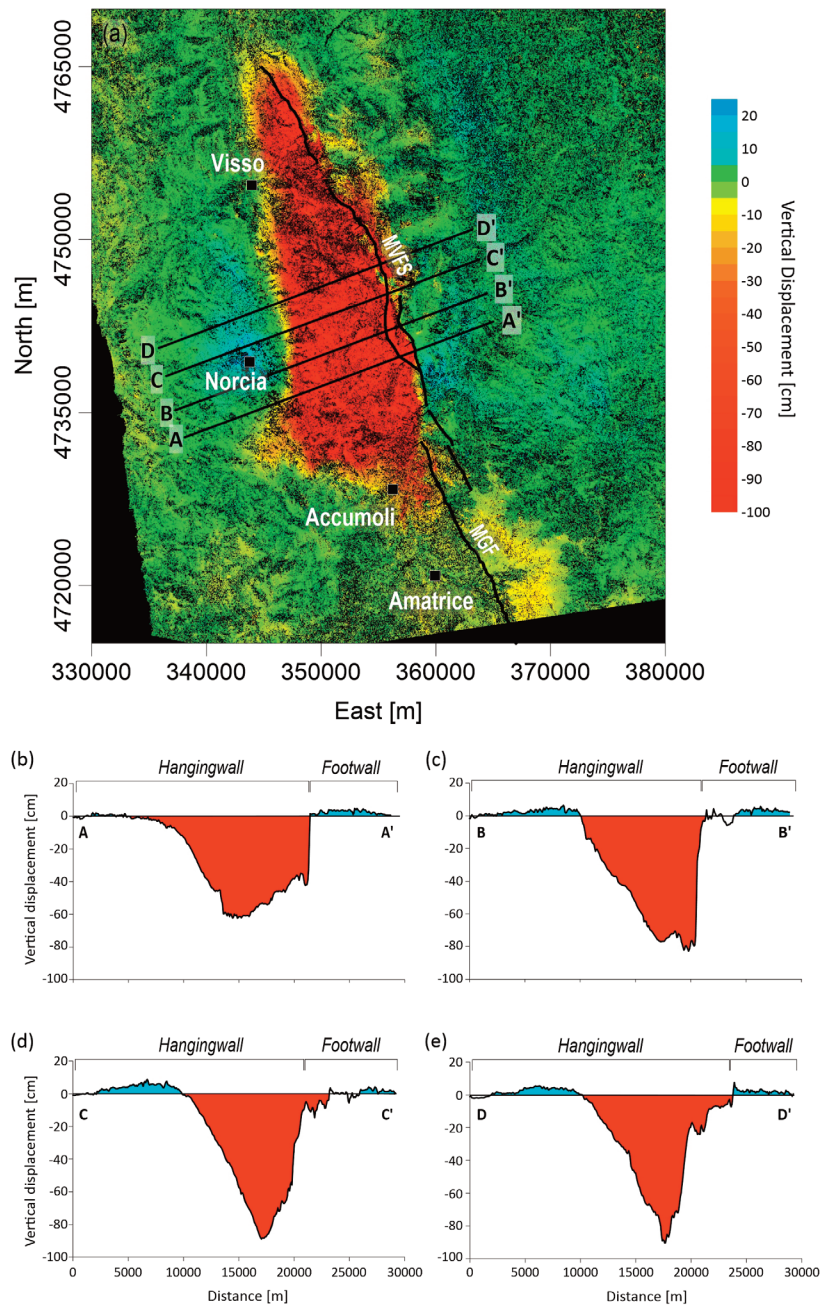


Figure 1. Four cross-sections of the ground motion generated by the Mw 6.5 Amatrice-Norcia 2016 (central Italy) seismic sequence [after Valerio et al., 2018]. For each section, the area of coseismic subsidence (red) is generally 10 times larger than the uplifted area (blue). The horizontal represents the pre-earthquake topography.

Graviquakes or normal fault earthquakes

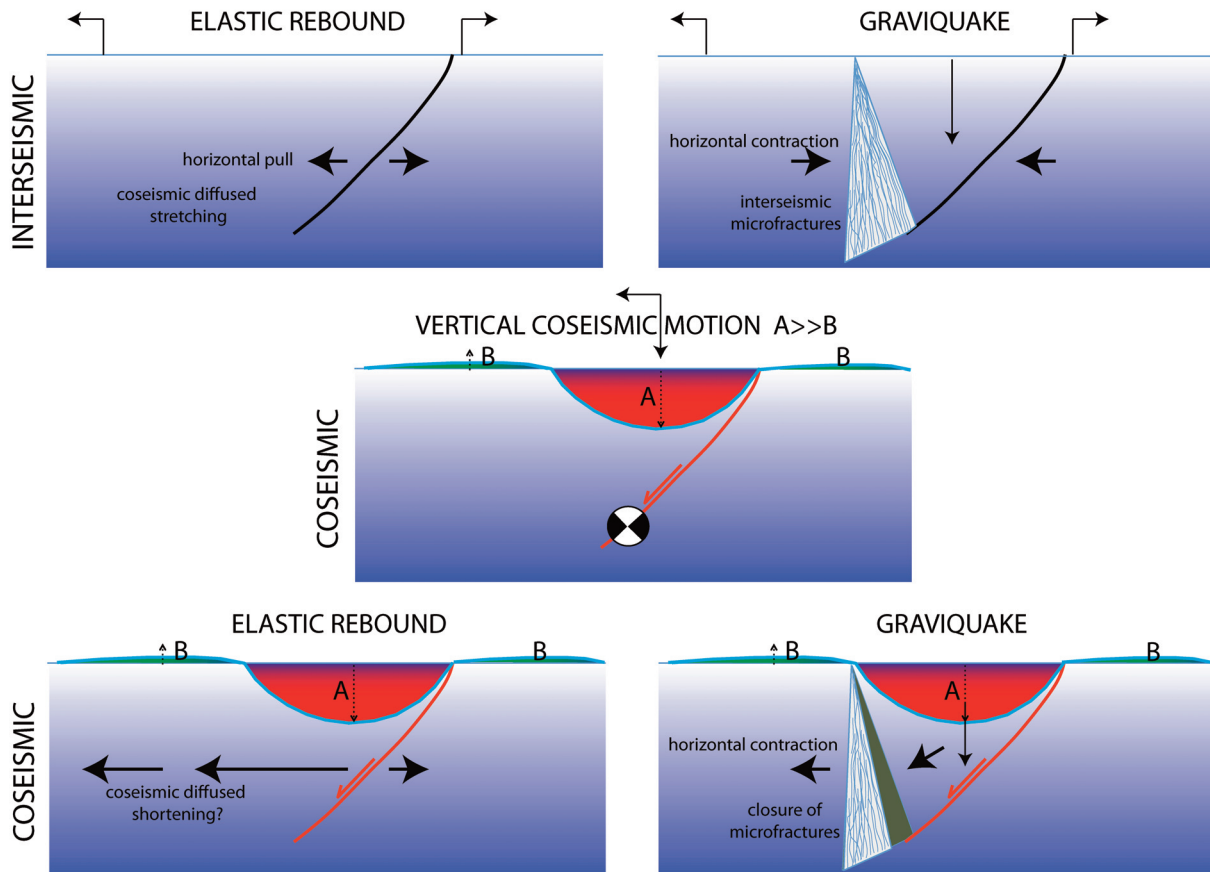


Figure 2. The elastic rebound and the gravitational collapse explain differently the asymmetry between the much larger coseismic subsidence associated to a normal fault earthquake, with respect to the uplifted volumes both in the hanging wall and footwall starting from the preparation phase during the interseismic period (above). In the middle panel are the observations, e.g., the vertical motion is larger than the coseismic horizontal shift recorded both by GPS and SAR. Below are the elastic rebound and the graviquake models at the coseismic stage.

2. Seismotectonic analysis

Segall and Heimisson [2019] claims that the larger coseismically subsided volume associated with the Mw 6.5 central Italy, 2016 earthquake is compatible with the elastic rebound theory, which models the crust as undergoing horizontal stretching, and explains the volume unbalance between larger coseismic subsidence (0.1 km^3) and much smaller uplift (0.01 km^3) as the result of diffuse larger elastic recall at depth. These authors argue against the model proposed by Bignami et al. [2019] who infer that this asymmetry in volume is generated by the closure of a pre-existing dilated volume developed during the interseismic period in the antithetic wedge with respect to the normal fault, and that the energy is provided by the gravitational collapse of the hanging wall.

As stated by Bignami et al. [2019], the coseismic slip affects an elastic medium and the asymmetry of the volumes can be computed also using the Okada [1985] analytical model, which satisfactorily reproduces the ground deformation (and its spatial distribution) with a given dip, slip and dimension of the normal fault surface. Indeed, the Okada model was applied to the 2016 event and acknowledged by Bignami et al. [2019]. Even though the Segall and Heimisson [2019] model partly replicates the Okada [1985] results, they calculated only the integral of the vertical movements that give the overall net difference between subsided and uplifted volumes, without any regard about the separated amount of these two volumes and their real (or approximate) ratio. The Segall and Heimisson [2019] formulation is therefore too simplified and much less precise than InSAR data that, on the contrary, have allowed calculating the ratio between the subsided and uplifted volumes. This is testified by the not negligible 20%

of discrepancy they found for the volume difference, which raises to 27% in our computation made with their technique. Hence, with this approach and numbers, they cannot confute the model proposed by Bignami et al. [2019]. Moreover, they compute the sum of the positive and negative uplift, without entering into the problem of where the ghost extra subsided volume disappears. Segall and Heimisson [2019] ignored the problem assuming high compressibility of the hanging wall or footwall, disregarding the real Poisson coefficient at crustal depth. Furthermore, they did not calculate in which volume this contraction should be accommodated in the hanging wall and at its bottom, close to the brittle-ductile transition. By the way, the compressibility should be allowed as well by a pre-existing dilation.

It is well established from the theory of mechanics of faulting [Anderson, 1951] that in extensional tectonic settings the maximum stress tensor (σ_1) is the lithostatic load (ρgz). Therefore, the main force moving the fault hanging wall is just gravity. Moreover, the pre-requisite for the Segall and Heimisson [2019] model is that, in extensional regimes, the crust is under horizontal tension, which is the case only above ~ 1 km depth [e.g., Twiss and Moores, 1992; Zoback, 2010] (Figure 3). This means that the differential stress has the minimum stress tensor (σ_3) positive below ~ 1 km depth, i.e., it is in compressive state. In these settings, the σ_3 is horizontal and therefore the crust is not undergoing tensile stress below 1 km depth (Figure 4). The vertical load (σ_1) is roughly stable, apart oscillations due to variable fluid pressure, atmospheric load, snow, etc. Rupture and faulting occur because, due to plates stretching, the minimum stress (σ_3) decreases through time, thus increasing the differential stress during the interseismic period, and enlarging the Mohr circle to the left, hence intercepting the Coulomb critical failure envelope or the Byerlee's law, which governs the process of frictional sliding, since the seismogenic fault is usually not a newly-formed shear fracture (Figure 5) [e.g., Carminati et al., 2020].

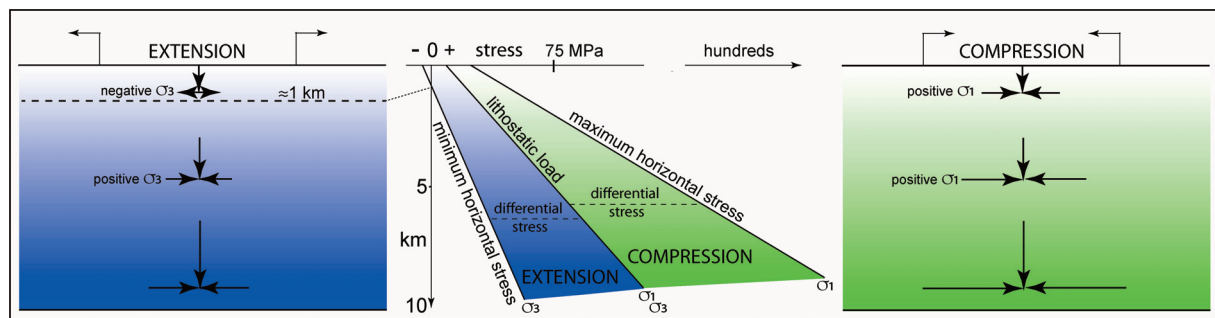


Figure 3. In extensional tectonic settings, the minimum stress tensor (σ_3) generates horizontal traction only above 1 km of depth, where it is negative. Below that depth it becomes positive, i.e., the crust is in compressive state even in rifting areas due to the increase of the confining pressure generated by the vertical, lithostatic load. Here an average density of 2.5 g/cm^3 and an increase of the lithostatic load of 25 MPa/km is assumed. The area between the lithostatic load and the minimum horizontal stress represents the deviatoric stress and contains the stress data measured in wells. To the right, the compressional tectonic setting in which contraction in the crust occurs also at shallow depth.

The other question is where does go the extra subsided volume. According to the general model supported by Segall and Heimisson [2019], this is accommodated by an elastic recovery associated with the horizontal rebound. Bignami et al. [2019] rather argued that the volume unbalance can be resolved only by a progressively dilated volume full of microfractures dominated by gravity, as suggested by SAR and GPS data showing coseismic displacement vectors with vertical component larger than horizontal.

The results of Segall and Heimisson [2019] assume a compressible Earth and the remarkable difference between subsidence and uplift is obtained for low Poisson's coefficients. For Poisson's coefficient (ν) approaching 0.5, this difference vanishes. However, the dominant lithology of the volume affected by the 2016 earthquake are carbonate rocks, characterized by a Poisson's coefficient that should increase with the confining pressure at depth. As inferred in triaxial conditions, at confining pressure of 150-400 MPa, equivalent to about 6-15 km depth, it could reach

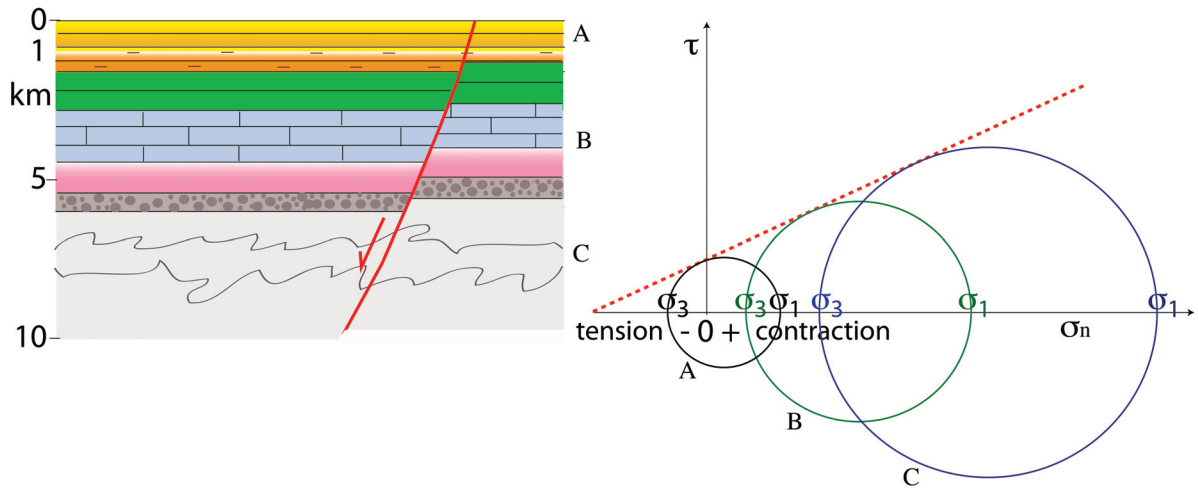


Figure 4. Three cases (A, B, C) with increasing depth and differential stress in extensional tectonic setting. The minimum stress tensor (σ_3) is negative (tension) only above about 1 km depth. Therefore, only the shallow circle A has σ_3 negative. Below 1 km it is positive (contraction). The maximum stress tensor (σ_1) is always vertical, and corresponds to the lithostatic load. The whole crust is in compressional state below about 1 km. Therefore, at the earthquake nucleation depth, the crust is under horizontal contraction even in extensional tectonic settings.

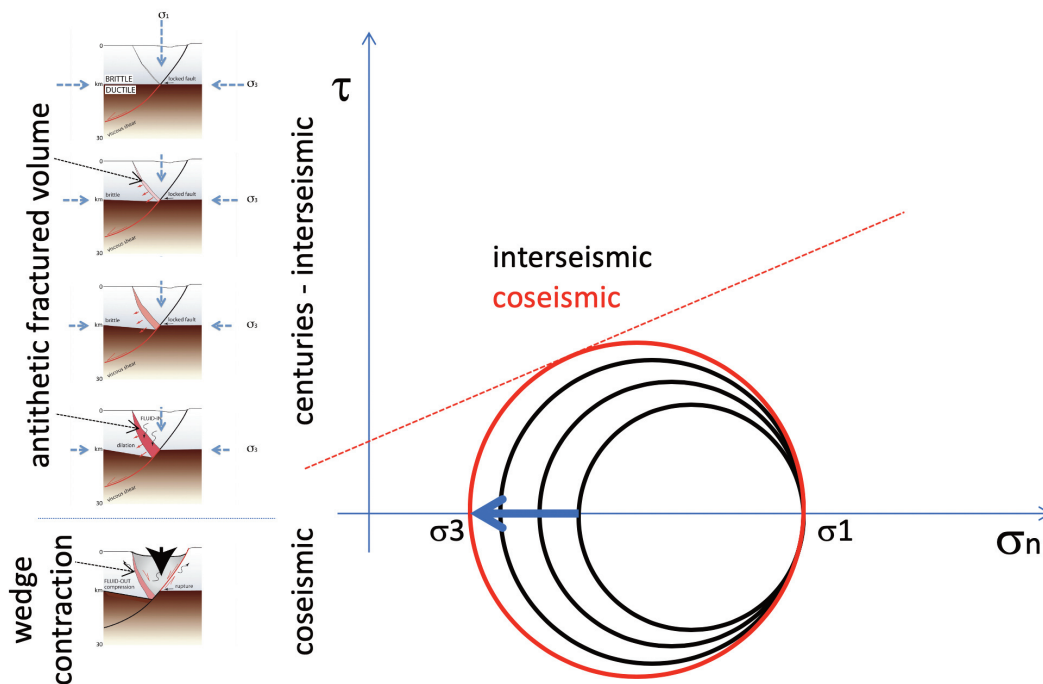


Figure 5. Notice that σ_1 , i.e., the vertical lithostatic load is fairly stable, whereas σ_3 is horizontal and decreasing during the interseismic period due to plate divergence, diminishing the confining pressure. The model infers the progressive formation of a dilated wedge permeated by microfractures in the brittle upper crust. The brittle-ductile transition dictates the strain partitioning and the switch between locked and unlocked normal fault in the cold, fragile upper crust. The antithetic wedge dilated during the interseismic period will eventually trigger the downfall of the hanging wall and the coseismic slip along the fault when the strength of the wedge and of the fault will not be anymore able to sustain the overlying weight. Bottom right, the Mohr diagram shows the evolution of the state of stress during the interseismic period, eventually evolving to the coseismic stage when the circle will intersect the Coulomb criterion, or more precisely it follows the Byerlee's law. This model agrees with the observation that in nature grabens are more frequently asymmetric or half-grabens. Modified after Carminati et al. [2020].

$\nu > 0.3-0.4$ [e.g., Al-Shayea 2004, its table 2], much larger than the Poisson's coefficient imposed by Segall and Heimisson [2019: $\nu = 0.25$] and required for the diffuse adjustment of their elastic rebound model. Madhubabu et al. [2016] measured $\nu = 0.39$ of carbonate rocks in uniaxial samples at the surface pressure, but with fast (few seconds) compression test as it is for earthquakes. Therefore, values of high ν are highly plausible and when assuming a Poisson's coefficient $\nu = 0.4$, the net volume decrease would be 0.03 km^3 , against the 0.10 km^3 of Bignami et al. [2019] estimate. The unbalanced ratio of 7.5 between subsided versus uplifted volumes described by Bignami et al. [2019] is only a minimum conservative value. Valerio et al. [2018] found a ratio up to 14 times (Figure 1). A lower Poisson coefficient of those rocks can be obtained only in presence of a multitude pre-existing millimetric fractures, which are visible in outcrops of tectonized carbonates and in boreholes. Thus, the volume unbalance is far from being resolved via elastic recovery associated with the horizontal rebound, whereas the extra volume of the hanging wall has to be allocated somewhere else. Also, in the semi-infinite half-space of Okada-like models, this unbalance can be accommodated far away from the fault surface. In the real Earth, GPS and SAR data rather indicate that the coseismic motion is confined within few tens of km away from the fault and the extra subsided volume must be compensated within that upper crustal brittle volume.

Rocks under compression may undergo pressure solution with related cleavage development, but this process does not occur instantaneously as required by the earthquake duration. Although the crust is under contraction even in extensional settings, fractures may form due to the lithostatic load. These fractures tend to parallel σ_1 and they may form as the positive σ_3 decreases in time due to the extensional tectonics, or because of compaction. Rocks under compression have much higher strength with respect to dilation, and once broken, they lose most of their elasticity.

3. Results

Valerio et al. [2018] demonstrated that a possible interpretation of the observed volumetric asymmetry related to the Mw 6.5 central Italy 2016 earthquake can be given through a numerical analysis showing the role of the hanging wall gravitational sliding. They proposed a 2D numerical model of the 2016 earthquake developed in a Finite Element (FE) environment under a structural-mechanic physic context. Specifically, this approach takes into account the linear elasticity behavior of the medium by considering the plain strain approximation mode. This aims to reduce the differences among the modelled vertical movements and those computed with the available ALOS-2 DInSAR measurements. In addition, in the numerical modelling, the tectonics and distribution of the seismicity in the study area are included, in order to account for the mechanical anisotropies and the active faults in the Apennines chain. We also specify that the Mw 6.5 2016 earthquake is not the first case study in which this approach has been applied, because it has already been successfully exploited for modeling other seismic sequences recorded in Central Italy [Tizzani et al. 2013; Lavecchia et al., 2016; Castaldo et al., 2018].

For sake of brevity, here we do not provide an extensive discussion on the applied numerical approach, which can be found in Tizzani et al. [2013]. We prefer to focus on the results of the simulated scenario accounting for the structural frameworks of the investigated area, which allows to retrieve the best fit coseismic deformation pattern. This consists of a SW-dipping normal fault and a conjugate antithetic dilated zone that may evolve into normal faults. See for example the ENE-dipping conjugate fault of the 2016 Amatrice-Norcia events that has been imagined both by hypocentral distribution of aftershocks, and it was mapped in the field [Galli et al., 2019a; 2019b; Improta et al., 2019; Galderisi and Galli, 2020]. Both structures lay above a low-angle ENE-dipping decollement (Figure 6a). The lithological setting is characterized by the following geological units having isotropic mechanical properties and constant densities [Valerio et al., 2018]: (i) a carbonate sedimentary succession (the Umbria-Marche stratigraphic sequence), (ii) an evaporitic layer above red beds and the underlying basement and (iii) a fractured limestone. The Earth's surface is the upper free boundary condition. In the numerical modeling we imposed a roller at the bottom and at the two lateral sides (Figure 6b). Further anisotropies generated by structural features are included. The gravity force is obviously applied as a body force in the whole model. The normal fault and of the antithetic zone in the hanging wall are modelled with frictional forces, whereas the low-angle ENE-dipping seismogenic layer as a roller boundary condition. We then add forces at the sides of the SW-dipping fault. In order to reproduce the coseismic displacement along the fault, the stationarity and linear elasticity approximation of the involved materials are assumed by considering the solution of the equilibrium mechanical equations [see Tizzani et al., 2013]. The result, accounting also for the topography of the considered area, shows a very good fit with the

Graviquakes or normal fault earthquakes

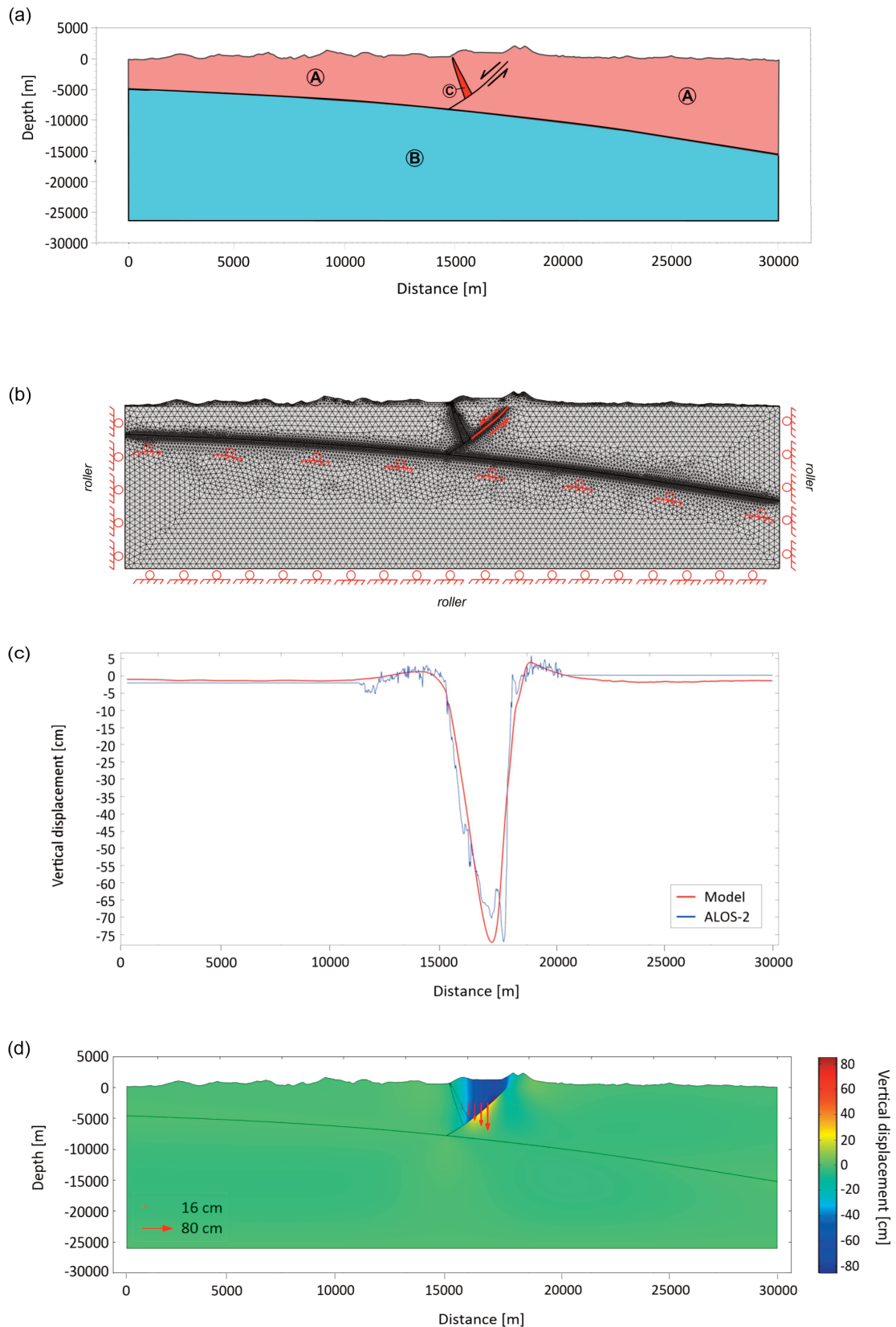


Figure 6. Numerical analysis results. (a) Simplified geological cross-section exploited in the considered FE environment; (b) discretized numerical domains with highlighted the boundary conditions. (c) Crustal distribution of the modeled vertical components of the retrieved displacements; the arrows indicate the modelled displacement vectors; (d) results of the SW-dipping fault and antithetic zone scenario. Comparison between the vertical component of the deformations retrieved through the DInSAR analysis and the FE modelling. Modified after Valerio et al. [2018].

surface deformation observed by the ALOS-2 DInSAR measurements (Figure 6c), [Valerio et al., 2018]. In addition, the crustal distribution of the modeled vertical displacement, derived by the optimization procedure (Figure 6d), highlights that the considered crustal wedge produced a significant modulation effect of the crustal displacement field that is coherent with the observed ground deformation. This analysis allows us to interpret the subsidence and uplift phenomena caused by the 2016, Mw 6.5 earthquake as the result of the gravitational motion of the hanging wall sliding along the normal fault and the frictional force acting in the opposite direction. This is coherent with the generation of the double couple along the fault plane recorded in the moment tensor, although its component may often be only partial [e.g., Miller et al., 1998]. The data analysis and the performed numerical models demonstrate that: (i) the coseismic uplift in the hanging wall block is about 1/14 of the subsidence, suggesting a strong volumetric asymmetry and unbalance between the subsided and the uplifted volumes within the upper crust, (ii) our 2D modelling highlights the presence of an antithetic zone as a prerequisite to reach the best fit between measured and simulated coseismic surface motions.

4. Discussion

The discussion in this article is not whether the brittle upper crust is elastic or not, but where the energy that generates normal fault earthquakes comes from and which is the main mechanical framework. These events dissipate energy, obviously in part by means of elastic waves in an elastic medium. However, normal fault earthquakes appear to be governed by different energy with respect to the other types of earthquakes. There are several differences between the seismicity of extensional tectonic settings with respect to strike-slip and compressive earthquakes that support a different origin for normal fault earthquakes with respect to the other tectonic settings, where the volume moves without vertical shift (transcurrent) or either against gravity (thrust). Here is a list of some relevant differences among normal faults and thrusts:

1. In extensional tectonic settings the σ_1 is the lithostatic load (gravity), whereas in compressive settings the σ_1 is the horizontal tectonic stress (elasticity);
2. At the global scale, the Gutenberg-Richter b-value is around 1.1 for normal faults, whereas is about 0.9 for thrusts [Schorlemmer et al., 2005], according to the lower maximum magnitude generated by normal fault earthquakes;
3. Normal fault-related earthquakes in crustal rifting areas have the maximum magnitude around 7.5, whereas thrusts may reach Mw 9.5;
4. Within the crust, the volumes involved by extensional faulting have a length about 3 times larger than the seismogenic thickness, which is usually the brittle-ductile transition or shallower decoupling surfaces, as in the Amatrice-Norcia 2016 seismic sequence. An example is Wasatch Fault in the central US, which is about 350-400 km long, but only segments in average 40-50 long ruptured [Machette et al., 1991]. Along compressive belts with high convergence rate (>6-7 cm/yr) this ratio may reach over 25 times (e.g., the 2004 Banda Aceh or the 2011 Tohoku Mw>9 events). In regions where the convergence rate is slower (few mm/yr), this ratio decreases to 2-4 times as well as the magnitude that can be up to Mw 6-7 (e.g., Italy accretionary wedges, [Petricca et al., 2018; 2019]);
5. With a given magnitude, the aftershocks of normal faults last longer than those of seismic sequences associated with thrusts [Valerio et al., 2017]. This is consistent with the contrast between the volume motion in favor or against gravity, respectively;
6. With a given magnitude, the stress drop of extensional earthquakes tends to be lower than that of compressive earthquakes [Cocco and Rovelli, 1989; Rovelli and Calderoni, 2014], which also supports the notion that rocks need more energy to move against gravity;
7. Compressive earthquakes nucleate more favorably at low lithostatic load (σ_3), i.e., low topography [Carminati et al., 2004], whereas extensional earthquakes increase their magnitude as the topography is higher and the lithostatic load (σ_1) increases;
8. Coseismic rupture tends to develop at depth and migrate upward along normal faults, whereas it preferably forms at shallow depth and migrates downward along thrust faults [Carminati et al., 2004];
9. Coseismic volumes are unbalanced, i.e., the normal faults earthquakes have the about 10 times larger extra volume accommodated at depth by the potential closure of fractures [Bignami et al., 2019], while thrusts

- account their larger uplifted volumes by the elastic rebound towards the free surface;
10. Earthquake magnitude increases with fault dip for normal faults, whereas it tends to be larger for a lower dip along thrust faults. The shallower the normal fault dip, the smaller the vertical gravitational movement and the shorter and slower the coseismic slip. The opposite can be observed for steeper normal faults.
 11. Fluids react oppositely when comparing extensional and compressive tectonic settings [Muir Wood and King, 1993; Doglioni et al., 2014; Barberio et al., 2017]; fluids are contained in fractures or primary porosity and their squeezing or recall requires contraction and dilation respectively as expected during the coseismic inversion in the two opposite settings; the pre-coseismic V_p/V_s ratio increase [Lucente et al., 2010] in extensional tectonic settings supports this interpretation. InSAR data provide an extremely precise coseismic amount and extent of subsidence, showing that it is the entire hanging wall volume that collapsed vertically [Bignami et al., 2019]; the macroseismic larger damages occurred in the area involved by the coseismic subsidence (near field), providing evidence of the influence of the vertical component of peak ground acceleration in weakening the strength of masonry buildings [Liberatore et al., 2019].

For all these reasons it has been suggested to classify earthquakes as a function of their source of energy, which is controlling the different phenomenology associated to normal faulting in favor of gravity (graviquake) and thrusting against gravity dominated by elastic energy (elastoquake) [Doglioni et al., 2015; Petricca et al., 2015; 2019]. The extensional seismicity of the Apennines is distributed along faults activated by volumes that, episodically, move brittle crustal prisms downward. The deformation gradually migrates over the whole seismogenic area undergoing tectonic extension. For example, the Norcia fault responsible for the 1703 sequence [Galli et al., 2018] was affecting a different volume to the west of the last 2016 seismic sequence.

5. Conclusions

Segall and Heimisson [2019] stated that the horizontal stretching is responsible for an elastic rebound during the earthquake and that the larger coseismically volume is elastically adsorbed in a compressible hanging wall. In turn, Bignami et al. [2019] suggest that the force is rather dictated by the gravitational potential, whereas the much larger coseismic subsidence with respect to the uplift can be explained by the abrupt closure at depth of a diffuse network of fractures, which progressively developed during the interseismic period.

It is worth noting that the elastic rebound model neglects either the strain partitioning between the upper brittle and the lower ductile portions of the crust, or the variations in competence of any further interlayered formations. Segall and Heimisson [2019] concluded the criticism to the Bignami et al. [2019] model claiming that geodetic data are consistent with elastic dislocation theory and do not require a volume collapse at depth. Conversely, in a number of papers [Doglioni et al., 2011; 2015; Bignami et al., 2019] it was emphasized the role of the brittle-ductile transition (BDT), or shallower decollements as the zone separating two different styles of interseismic deformation during the preparatory phase of an earthquake. A dilated wedge is kinematically required in the upper cold crust because normal faults are locked, whereas the lower crust is permanently shearing. This is a prerequisite in accommodating the collapsing volume during a normal fault earthquake.

Moreover, the dilated wedge should be populated by thousands of millimetric fractures filled by fluids as suggested by magnetotelluric surveys and higher V_p/V_s ratio. The search of those fractured volumes may illuminate where will be the next major seismic sequences.

The claimed Occam razor is in favor of the simplest explanation for the activation of normal fault earthquakes, which in this case is the force of gravity (Figure 7). The gravity force is absent in the Segall and Heimisson [2019] equations. The horizontal tensional stress (negative σ_3) they invoke in extensional settings does not exist, and therefore the model of the elastic rebound as related to the horizontal stretching for generating normal fault earthquakes is simply not correct. The volume dimension in the hanging wall of normal faults has in average a length three times bigger than the seismogenic thickness above the brittle-ductile transition or shallower decollements. This limits the fault plane dimension and the earthquake magnitude (Figure 8). Internal friction of the crust is determined by lithology and fluids pressure. Low friction rocks generate low-angle normal faults that produce creep and low magnitude earthquakes. High-friction rocks rather generate steep faults and higher magnitude seismicity (Figure 9).

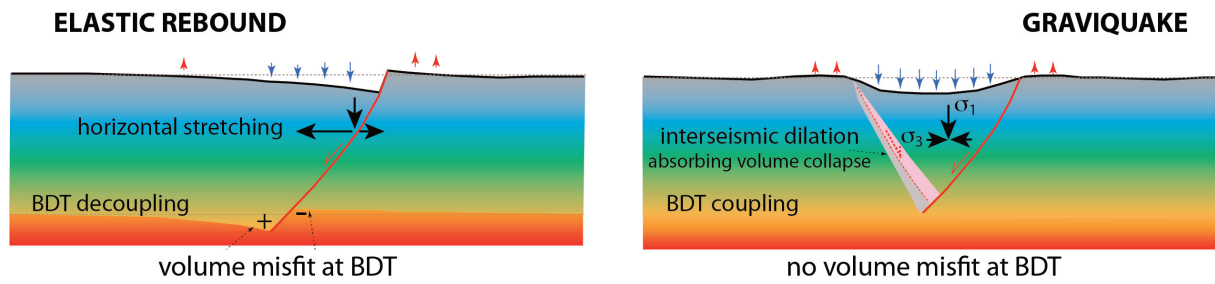


Figure 7. Comparison between the coseismic model of elastic rebound and graviquake for normal faulting (BDT, brittle-ductile transition). In the elastic rebound, the larger subsided volume is compensated by the diffuse horizontal contraction in the hanging wall or by the dissipation of the volume outside the section, being required a decoupling at the brittle upper crust base where the differential stress for rupture is maximum. In the graviquake model, the extra volume is rather adsorbed by an interseismic pre-dilated wedge. The hanging wall moves primarily downward, as dictated by the lithostatic load σ_1 . Since the horizontal pull is missing below 1 km, the coseismic dominant motion is not horizontal but rather vertical, and the maximum stress tensor is given by the lithostatic load; therefore, we consider the graviquake model more realistic.

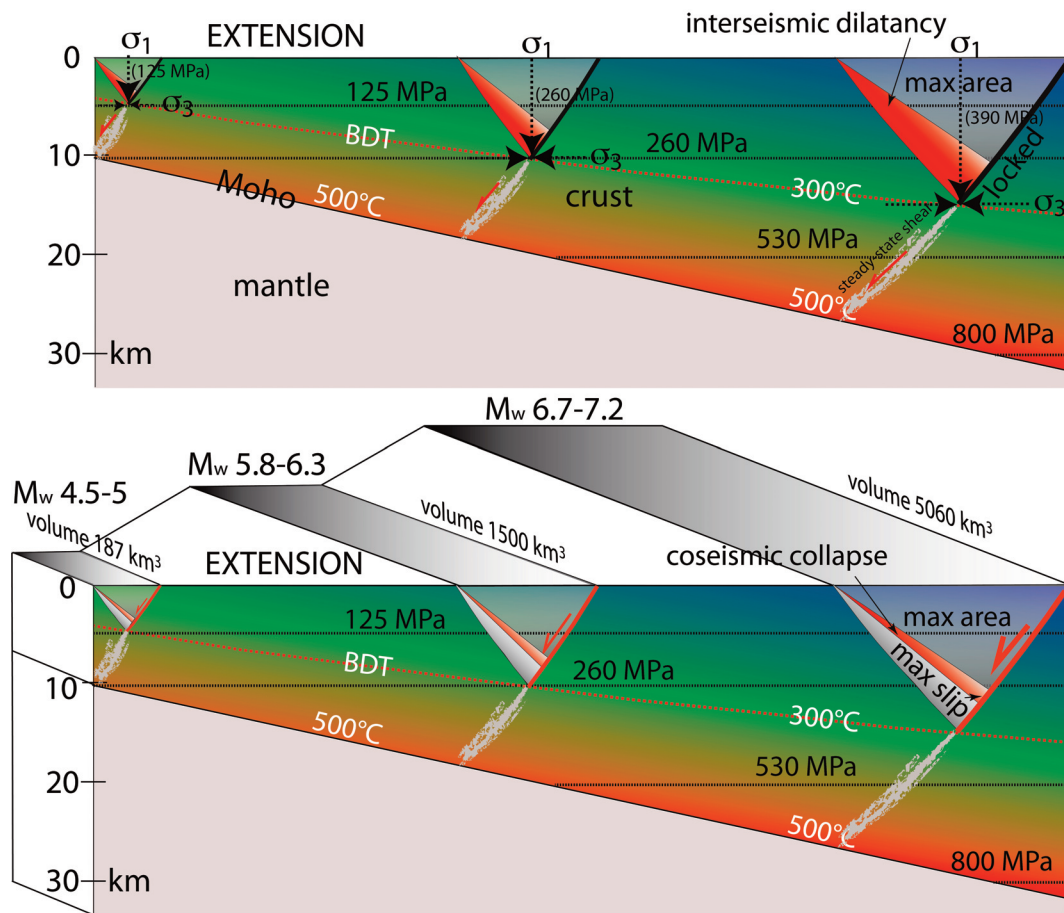


Figure 8. In extensional tectonic settings, the ratio between the seismogenic layer depth and the hanging wall length appears to be, in average, $3(\pm 1)$. As the thickness increases, the volume enlarges, the fault is longer, and the hanging wall collapse determines a greater fault slip and a consequent higher earthquake magnitude. Note that doubling the seismogenic layer from 5 to 10 km, the volume increases about 1 order of magnitude, as the maximum earthquake size, from M_5 to M_6 . BDT, brittle-ductile transition. The red wedges in the section above suggest the inferred dilated crustal volume permeated by thousands of millimetric microfractures.

Graviquakes or normal fault earthquakes

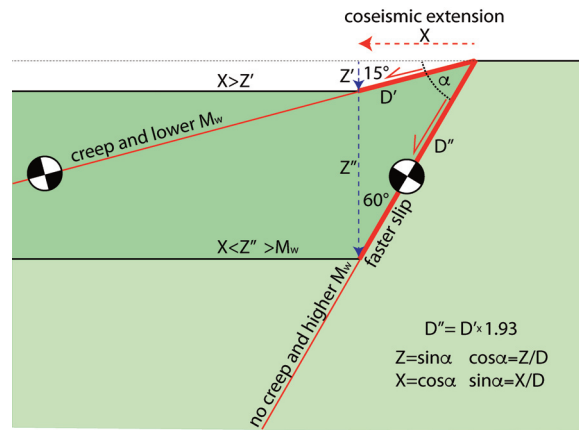


Figure 9. Assuming a coseismic horizontal extension X , the vertical component varies as a function of the dip (α) of the normal fault. Two cases are shown, a 15° and 60° respectively. The vertical component Z' of 15° is smaller than the horizontal motion, whereas with a fault dip of 60° the vertical component Z'' is larger than X . $X=Z$ if the fault dip is 45° . The fault displacement of the 15° (D') is about half of the 60° (D''). The low dip is usually a consequence of low friction rocks and is associated to creeping faults generating low magnitude earthquakes. During coseismic stage, the small slip and vertical component determine slower slip. The steeper dip is rather related to high friction lithologies, low or no creep and higher magnitude seismicity. This can be explained by the longer vertical component (Z'') and higher gravitational potential, the larger displacement (D'') which imply also a faster motion along the fault. This framework is consistent with the mechanical constraints given by the vertical σ_1 dominating the source of energy, i.e., gravity within an extensional tectonic setting.

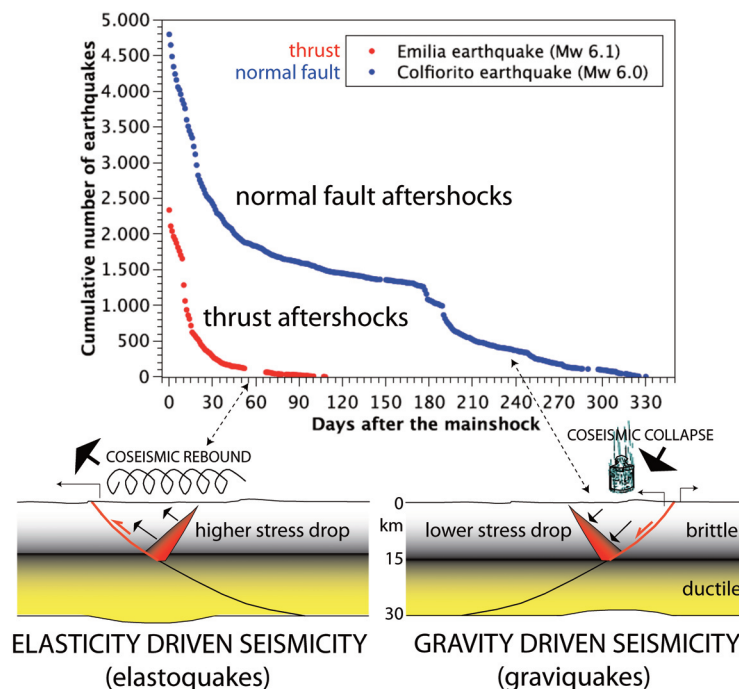


Figure 10. Above, comparison of the number and duration of aftershocks of normal vs thrust faults related to two Italian earthquakes (Colfiorito 1997; Emilia 2012). The same magnitude of completeness was used ($M_c 2.5$). Normal fault aftershocks are much more numerous and last longer. This can be interpreted as related to the motion in favor of gravity and the sequence will last when the final gravitational equilibrium is reached. Along thrust faults, the motion against gravity inhibits and buffers most of the further motion after the mainshock. Therefore the two sequences can be inferred as earthquakes delivering gravitational and elastic energy, respectively, and for this reason they should be distinguished into graviquakes and elastoquakes (below).

In spite of a smaller maximum magnitude, normal faults earthquakes are followed by a large number of aftershocks with respect to thrust related events [Valerio et al., 2017], this being compatible with the motion in favor of gravity (Figure 10). Normal faults rupture as soon as the hanging wall can slide down when the lithostatic load overcomes the fault friction and the conjugate interseismically dilated wedge is present to accommodate the extra volume at depth. The gravitational energy can explain the lower volumes and magnitude of earthquakes associated to normal faults with respect to those moving against gravity [Doglioni et al., 2015] as shown in Figure 11. The hanging wall does not fall into a giant cave below, but it is obviously re-closing an intensely fractured rock volume like closing an accordion. The fundamental process governing stick-slip behavior holds and is frictional sliding, but the energy comes from the lithostatic load and can occur because of the deep presence of the pre-stretched upper crust. This can explain why magnitude of normal fault earthquakes increases with dip, whereas it decreases for thrust-related events as shown in Figure 12. Last but not least, the search for the fractured volume in the antithetic zone of forthcoming normal fault activation may represent a relevant target of investigation by tomography and magnetotelluric analysis, providing a clue for the areas more prone to seismic activation.

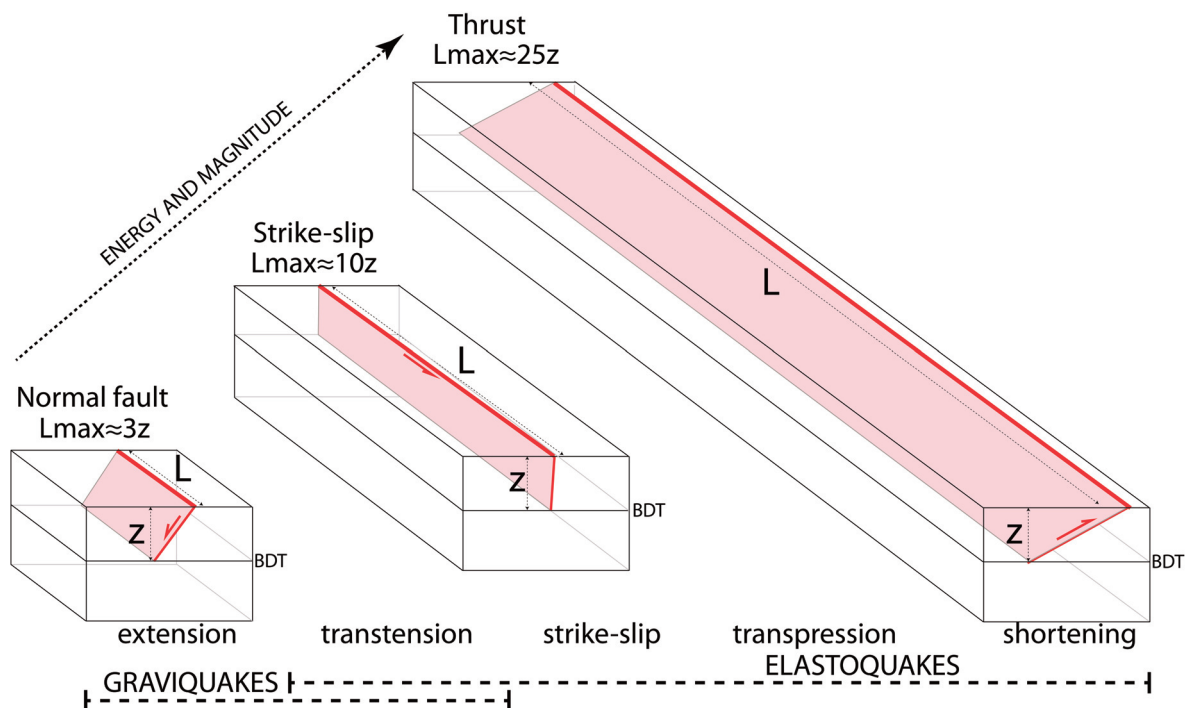


Figure 11. Classification of earthquakes as a function of the energy source. Normal fault earthquakes are controlled mainly by gravity and the hanging wall moves downward as soon as it can slide, involving smaller volumes with respect to strike-slip and thrust faults that can move only when the threshold of the friction and rigidity are overtaken by the elastic energy accumulated during the interseismic period. Note that the volume and fault length (L) is about 3 times the seismogenic layer thickness (z) for normal faults, increasing to possibly more than 25 times in megathrust earthquakes. This is consistent with the higher magnitude that can be reached by thrusts that move against gravity with respect to normal faults that move in favor of gravity.

Acknowledgements. Thanks to Matteo Albano, Salvatore Barba and Paolo Galli for useful discussions and two anonymous reviewers for their constructive critical reading.

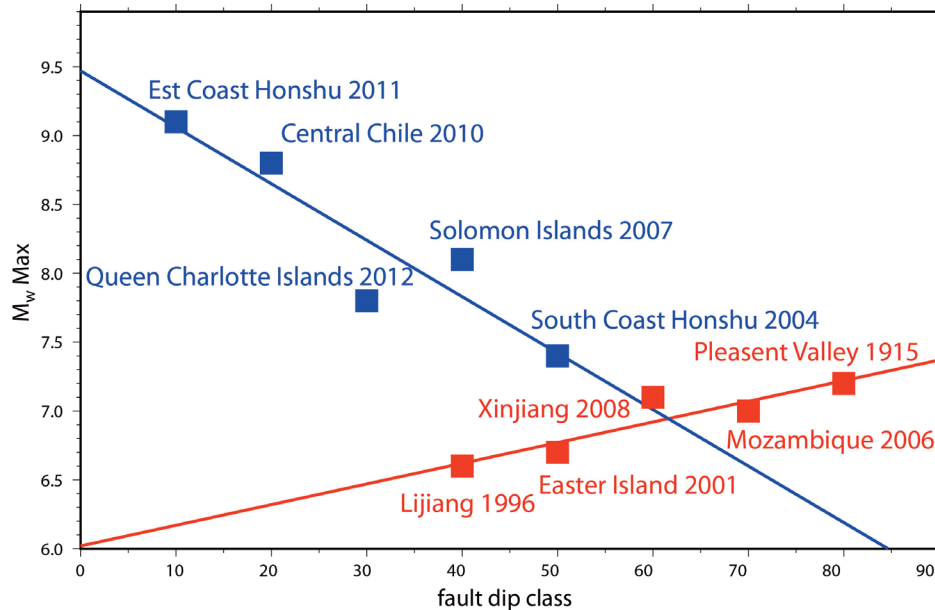


Figure 12. Comparison between thrust-related (blue) and normal fault earthquakes (red) versus fault dip. The magnitude decreases with dip for thrusts, whereas it increases along normal faults. This opposite behavior supports different energy supply for the two tectonic settings, i.e., elastic rebound for moving the hanging wall upward against gravity, and gravitational potential for normal faults.

References

- Al-Shayea, N. A. (2004). Effects of testing methods and conditions on the elastic properties of limestone rock. *Engi. Geol.*, 74(1-2), pp.139-156.
- Anderson, E. M. (1951). *The dynamics of faulting and dyke formation with applications to Britain*. Hafner Pub. Co.
- Barberio, M. D., M. Barbieri, A. Billi, C. Doglioni, M. Petitta (2017). Hydrogeochemical changes before and during the 2016 Amatrice-Norcia seismic sequence (central Italy). *Sci. Reps.*, 7, 11735, <https://doi.org/10.1038/s41598-017-11990-8>
- Biglami, C., E. Valerio, E. Carminati, C. Doglioni, P. Tizzani (2019). Volume unbalance on the 2016 Amatrice - Norcia (central Italy) seismic sequence and insights on normal fault earthquake mechanism. *Sci. Reps*, 9:4250, doi: <https://doi.org/10.1038/s41598-019-40958-z>
- Carminati, E., C. Doglioni and S. Barba (2004). Reverse migration of seismicity on thrusts and normal faults. *Earth Sci. Rev.*, 65, 195–222.
- Carminati, E., C. Biglami, C. Doglioni and L. Smeraglia (2020). Lithological control on multiple surface ruptures during the 2016-2017 Amatrice-Norcia seismic sequence. *J. Geod.*, 134, 101676, <https://doi.org/10.1016/j.jog.2019.101676>
- Castaldo, R., R. de Nardis, V. De Novellis, F. Ferrarini, R. Lanari, G. Lavecchia, S. Pepe, G. Solaro and P. Tizzani (2019). Coseismic Stress and Strain Field Changes Investigation Through 3-D Finite Element Modeling of DInSAR and GPS Measurements and Geological/Seismological Data: The L'Aquila (Italy) 2009 Earthquake Case Study. *J. Geophys. Res.: Solid Earth*, 123. <https://doi.org/10.1002/2017JB01445>
- Cocco, M. and A. Rovelli (1989). Evidence for the Variation of Stress Drop Between Normal and Thrust Faulting Earthquake in Italy. *J. Geophys. Res.* 94, B7, 9399-9416.
- Doglioni, C., S. Barba, E. Carminati and F. Riguzzi (2011). Role of the brittle-ductile transition on fault activation. *Phys. Earth Planet. Int.*, 184, 160–171.

- Galderisi, A., and P. Galli (2020). Offset components and fault-block motion during the 2016 Central Italy earthquake (Mw 6.6, Monte Vettore Fault System). *J. Struct. Geol.*, 134, <https://doi.org/10.1016/j.jsg.2020.104014>
- Galli, P., A. Galderisi, I. Iardo, S. Piscitelli, V. Scionti, J. Bellanova and F. Calzoni (2018). Holocene paleoseismology of the Norcia fault system (Central Italy). *Tectonophysics*, 745, 154-169.
- Galli, P., A. Galderisi, E. Peronace, B. Giaccio, I. Hajdas, P. Messina, D. Pileggi and F. Polpetta (2019a). The awakening of the dormant Mount Vettore fault (2016 central Italy earthquake, Mw 6.6): Paleoseismic clues on its millennial silences. *Tectonics*, 38(2), 687-705.
- Galli, P., A. Galderisi, S. Martino, G. Scarascia Mugnozza and F. Bozzano (2019b). The coseismic faulting of the San Benedetto tunnel (2016, Mw 6.6 central Italy earthquake), *Tunnels and Underground Cities*. In: *Engineering and Innovation meet Archaeology, Architecture and Art – Peila, Viggiani & Celestino (Eds)*, Taylor & Francis Group, London.
- Improta, L., D. Latorre, L. Margheriti, A. Nardi, A. Marchetti, A.M. Lombardi, B. Castello, F. Villani, M.G. Ciaccio, F.M. Mele and M. Moretti (2019). Multi-segment rupture of the 2016 Amatrice-Visso-Norcia seismic sequence (central Italy) constrained by the first high-quality catalog of Early Aftershocks. *Sci. Reps.*, 9(1), 1-13.
- Lavecchia, G., R. Castaldo, R. de Nardis, V. De Novellis, F. Ferrarini, S. Pepe, F. Brozzetti, G. Solaro, D. Cirillo, M. Bonano, P. Boncio, F. Casu, C. De Luca, R. Lanari, M. Manunta, M. Manzo, A. Pepe, I. Zinno and P. Tizzani (2016). Ground deformation and source geometry of the 24 August 2016 Amatrice earthquake (Central Italy) investigated through analytical and numerical modeling of DInSAR measurements and structural-geological data. *Geophys. Res. Lett.*, 43, 24, 28, 12,389–12,398
- Liberatore, D., C. Doglioni, O. Al Shawa, S. Atzori and L. Sorrentino (2019). Effects of coseismic ground vertical motion on masonry constructions damage during the 2016 Amatrice-Norcia (Central Italy) earthquakes. *Soil Dyn. Earthq. Eng.*, 120 (2019) 423-435, <https://doi.org/10.1016/j.soildyn.2019.02.015>
- Machette, M.N., S.F. Personius, A. R. Nelson, D. P. Schwartz and W. R. Lund (1991). The Wasatch fault zone, Utah-Segmentation and history of Holocene earthquakes. *J. Struct. Geol.*, 13(2),137-149.
- Madhubabu, N., P. K. Singh, A. Kainthola, B. Mahanta, A. Tripathy and T.N. Singh (2016). Prediction of compressive strength and elastic modulus of carbonate rocks. *Measurement*, 88, 202-213.
- Miller, A. D., G.R. Foulger and B R. Julian (1998). Non-double-couple earthquakes 2. Observations. *Rev. Geophys.* 36, 4, 551-568.
- Muir-Wood, R. and G.C.P. King (1993). Hydrological signatures of earthquake strain. *J. Geophys. Res.* 98, (B12), 22035-22068, <https://doi.org/10.1029/93JB02219>
- Okada, Y. (1985). Surface Deformation Due to Shear and Tensile Faults in a Half-Space. *Bull. Seism. Soc. Am.*, 75, 1135–1154.
- Petricca P., S. Barba, E. Carminati, C. Doglioni and F. Riguzzi (2015). Graviquakes in Italy. *Tectonophysics*, 656, 202–214, [doi:10.1016/j.tecto.2015.07.001](https://doi.org/10.1016/j.tecto.2015.07.001)
- Petricca, P., E. Carminati, C. Doglioni and F. Riguzzi (2018). Brittle-ductile transition depth versus convergence rate: impact on seismicity. *Phys. Earth and Planet. Int.*, <https://doi.org/10.1016/j.pepi.2018.09.002>
- Petricca P., E. Carminati and C. Doglioni (2019). The Decollement Depth of Active Thrust Faults in Italy: Implications on Potential Earthquake Magnitude. *Tectonics*, 38, <https://doi.org/10.1029/2019TC005641>
- Rovelli, A. and G. Calderoni (2014). Stress drops of the 1997–1998 Colfiorito, Central Italy earthquakes: hints for a common behaviour of normal faults in the Apennines. *Pure and App. Geophys.*, 171(10), pp.2731-2746.
- Schorlemmer, D., S. Wiemer and M. Wyss (2005). Variations in earthquake-size distribution across different stress regimes. *Nature* 437, 22.
- Segall, P. and E. R. Heimisson (2019). On the Integrated Surface Uplift for Dip-Slip Faults. *Bull. Seism. Soc. Am.*, 109, 6, 2738–2740, <http://doi.org/10.1785/0120190220>
- Stein, S. and M. Wysession (2009). *An introduction to seismology, earthquakes, and earth structure*. John Wiley and Sons.
- Tizzani, P., R. Castaldo, G. Solaro, S. Pepe, M. Bonano, F. Casu, M. Manunta, M. Manzo, A. Pepe, S. Samsonov, R. Lanari, and E. Sansosti (2013). New insights into the 2012 Emilia (Italy) seismic sequence through advanced numerical modeling of ground deformation InSAR measurements. *Geophys. Res. Lett.* 40 (10), 1971-1977.
- Twiss, R. J., and E.M. Moores (1992). *Structural geology*. W. H. Freeman & Co., San Francisco, 532.
- Valerio, E., P. Tizzani, E. Carminati and C. Doglioni (2017). Longer aftershocks duration in extensional tectonic settings. *Scientific Reports*, 7, 16403, <https://doi.org/10.1038/s41598-017-14550-2>

Graviquakes or normal fault earthquakes

- Valerio, E., P. Tizzani, E. Carminati, C. Doglioni, S. Pepe, P. Petricca, C. De Luca, C., Bignami, G. Solaro, R., Castaldo, V. De Novellis and R. Lanari (2018). Ground Deformation and Source Geometry of the 30 October 2016 Mw 6.5 Norcia Earthquake (Central Italy) Investigated Through Seismological Data, DInSAR Measurements, and Numerical Modelling. *Remote Sensing*, 10, 1901, <https://doi.org/10.3390/rs10121901>
- Zoback, M.D., (2010). *Reservoir geomechanics*. Cambridge: Cambridge University Press, <https://doi.org/10.1017/CBO9780511586477>

*CORRESPONDING AUTHOR: Carlo DOGLIONI,

Istituto Nazionale di Geofisica e Vulcanologia,

Rome, Italy;

Dipartimento di Scienze della Terra,

Sapienza University, Rome, Italy

e-mail carlo.doglioni@ingv.it

© 2020 the Istituto Nazionale di Geofisica e Vulcanologia.

All rights reserved